arXiv:1702.05389v1 [cond-mat.mes-hall] 17 Feb 2017

Magnetic control of heat and charge transport in a paramagnetic molecular dimer

J. D. Vasquez Jaramillo and J. Fransson*
Department of Physics and Astronomy, Box 516, 75120, Uppsala University, Uppsala, Sweden
(Dated: February 20, 2017)

Utilizing the possibility to electrically and thermally control the magnetic exchange interactions between localized magnetic moments, we here present results regarding the charge and heat transport properties in dimer comprising, for example, paramagnetic molecules. We consider both charge and heat transport under non-equilibrium conditions imposed using voltage bias and temperature difference across the junction. Generic properties for both transport quantities are reduced currents in the magnetically active regime compared to the inactive, or, paramagnetic, and efficient current blockade in the anti-ferromagnetic regime. In contrast, while the charge current is about an order of magnitude larger in the ferromagnetic regime, compared to the anti-ferromagnetic, the heat current is efficiently blockaded there as well. This disparate behavior of the heat current is attributed to current resonances in the ferromagnetic regime which counteract the normal heat flow. It can also be noted that the temperature difference has a strongly reducing effect of the exchange interaction, which tends to destroy the magnetic control of the transport properties. The upside of the weakened exchange interaction is a possibility to tune the system into thermal rectification, for both the charge and heat currents.

I. INTRODUCTION

Thermal transport properties in molecular junctions can be of electronic origin or mediated through lattice vibrations [1]. There has been an increasing interest in the study of thermal properties in molecular junctions [2–5], stimulated by experimental observations [2], where several realizations of tunneling junctions consisting of noble metal electrodes coupled to polymers that absorb, emit, and transmit heat have been reported [4, 6]. The interest is, moreover, driven from the perspective of information science and technology with respect to entropy production [3, 7] and the meaning of the thermodynamics in low dimensional systems [3, 8–10]. This was motivated by the discovery of conducting polymers and solitonic electronic transport mechanisms discovered by Hideki Shirakawa, see [11] and references therein, from where polyacetylene became the test bench, that bridged the gap between organic and inorganic chemistry regarding electronic transport [12–14]. Since then, charge transport has been extensively studied theoretically and experimentally in molecular junctions [15–25]. From the same standpoint, thermal transport studies were conceived and came to be conclusive in the upcoming years [2]. Subsequently, several theoretical studies demonstrated the possibility to conduct both heat and charge through tunneling junctions [26–35], both in presence and absence of lattice vibrations, always fulfilling the thermodynamic definitions used to define transport properties when downsizing these devices, where the thermodynamic limit breaks [8, 9, 36].

Moreover, the simultaneous analyses of electronic and thermal transport properties in molecular junctions [37, 38], provide the necessary framework to determine the Lorenz number and whether the Weideman-Franz law remains true for specific interactions in the molecular junction [39, 40]. Furthermore, the analysis of the universality of the Lorenz number in relation to the corresponding Seebeck coefficient plays a crucial role in the understanding of the nature and emergence of decoherence in the system of study. For these reasons, at least, the study of thermal transport in molecular junctions is of great importance and relevance not only from the perspective of device modeling, but as well when looking at the problem of measurement and coherence in molecular junctions [41–43].

Recently it has been also demonstrated that electric field control, through a gate electrode in three terminal devices, of interfering transport pathways is possible using single molecule transistor based on anthraquinone molecules [44, 45]. The electric field can change conjugation of π electrons which is believed to be responsible for quantum decoherence [43, 46–50] in this type of set-up. Therefore, lifting the destructive quantum interference which is seen in the transmission of the junction, as reported in different theoretical [43, 50–52] and experimental [46, 47, 49, 53] studies performed on linearly and cross-conjugated organic molecules, as well as with molecules exhibiting broken conjugation [46, 47]. The possibility to control the conjugation by inducing a reduction in the organic molecule through an electric field exploits the possibility to use solid state devices as gate electrodes [44] to control electrical and thermal properties in this type of junction rather than using electrochemical control [54].

Recent theoretical advances have demonstrated the possibility to perform all electrical control in molecular junctions to both read and write spin states in two site molecular bridges [55, 56]. In particular is was theoretically predicted that the electronically mediated indirect exchange interaction between the localized spins can be employed to control the charge transport properties [55, 56]. The same type of all electrical control has been also demonstrated in [6], where the direct electric control is used to manipulate the spin ground state of a single metal complex, imposing a transition from a high spin configuration ($S = 5/2$) to a low spin configuration ($S = 1/2$) in a three terminal device. The type of system studied in [55, 57], consists of two single level molecules in contact with a paramagnetic molecule each of them, embedded in a non-ferromagnetic metallic tunneling junction, where

*Electronic address: Jonas.Fransson@physics.uu.se

the two paramagnetic molecules exhibiting a macro spin interact with each other isotropically through electronically mediated indirect exchange interaction. It was shown the effective exchange interaction comprise both isotropic Heisenberg-like and anisotropic Ising- and Dzyaloshinski-Moriya-like interactions, and that these can all be tuned and controlled even far from equilibrium conditions either by gate and/or bias voltages or thermally through a temperature difference across the junction [57]. This particular configuration allows controlled manipulations of the spin state that may be applicable as a read and write device [55], due to appreciable effects on the electric transport properties with respect to the local spin configurations.

A particular application to spin dynamics of a single molecular magnet is studied in [58, 59], where the the magnet is driven externally by an external magnetic field, and the system of study is described by an effective spin model, that has the form of the Hamiltonian model used in [57]. Besides the problem of transport [15, 25, 60] and measurement [61, 62] in tunneling junctions, the study of decoherence and entanglement emerges as an important problem [43, 50, 63, 64], intimately related with entropy production and heat flow through the junction, both controlled electrically and thermally as suggested in [57], and both of them completely unexplored for the configuration proposed in [55].

Here we build on the previous predictions made in [55, 57] for dimers of magnetic molecules in which the effective spin-spin interactions are mediated by the properties of the delocalized electrons and extend to thermally induced magnetic configurations, and charge and thermal transport properties. The set-up pertains to, for instance, M-phthalocyanine (MPc), M-porphyrins, where M denotes a transition metal atom [65–68], e.g., Cr, Mn, Fe, Co, Ni, Cu, but also bis(phthalocyaninato)R (TPc_2) [69, 70], where R denotes a rare earth element, e.g., Tb, and can be realized in, for example, mechanically controlled break-junctions [70, 71], in carbon nanotube assemblies [69] and scanning tunneling microscope [66, 67].

We consider heat and charge transport as the result of the electrothermal control of the junction, that is, we investigate the charge and heat conductance with respect to the bias voltage and thermal gradient across the junction. With this background we proceed and consider a non-equilibrium Seebeck coefficient defined as the ratio between the differential conductances with respect to the thermal gradient and bias voltage [72]. In addition, we consider an *energy Seebeck coefficient*, analogously defined for the heat differential conductances. Our predictions and results are based on non-equilibrium Green functions defined on the Keldysh contour.

Throughout this study we consider spin degenerate conditions in that we assume non-magnetic metals in the leads as well as the absence of externally applied magnetic fields. The advantage with this set-up, compared to designs based on ferromagnetic leads is that the dipolar and quadrupolar fields considered in Ref. [73] here becomes vanishingly small. Therefore the effective isotropic electron mediated spin-spin interactions dominates the properties and control of the molecular dimer. In this sense, our system would serve as a representation of paramagnetic spintronics, or *paratronics*.

The paper is organized as follows. We define the type of system in Sec. II and proceed in Sec. III to discuss our approach to the transport calculations. Then, in Sec. IV we survey and discuss our results while the paper is summarized in Sec. V.

II. MAGNETIC MOLECULAR DIMER IN A JUNCTION

The specific set-up we address in this article comprises a dimer of paramagnetic molecules which are embedded in series in the junction between normal metallic leads, see Fig. 1 (a). The paramagnetic molecules consist of a ligand structure which sp-orbitals define the spin-degenerate HOMO or LUMO orbitals pertaining to the present investigation and a localized spin moment. We assume that the d-, or, f-levels have a small hybridization with the sp-orbitals and are sufficiently localized to allow to consider the spin moment in the localized moment picture, in which the localized moment only interacts with the de-localized electrons via exchange. Having such systems in mind, also justifies that we neglect spin-orbit coupling in the molecular orbitals, since such coupling essentially pertains to the localized electrons constituting the paramagnetic moment, and also that we consider the molecular levels in a single particle form, which is justified for for s- and p-electrons. The molecular orbitals couple via tunneling both to one another and to the adjacent lead.

We model this set-up using the Hamiltonian

$$\mathcal{H} = \mathcal{H}_M + \mathcal{H}_{\rm int} + \mathcal{H}_L + \mathcal{H}_R + \mathcal{H}_T. \tag{1}$$

Here, the molecular HOMO or LUMO levels are defined by

$$\mathcal{H}_M = \sum_\sigma \left(\sum_{m=L,R} \varepsilon_m d^\dagger_{m\sigma} d_{m\sigma} + \mathcal{T}_c (d^\dagger_{L\sigma} d_{R\sigma} + H.c.) \right), \tag{2}$$

where $d^\dagger_{m\sigma}$ ($d_{m\sigma}$) creates (annihilates) an electron in the left (L) or right (R) molecule at the energy $\varepsilon_m = \varepsilon_0$ and spin $\sigma = \uparrow, \downarrow$, whereas $\mathcal{T}_c$ defines the tunneling rate between the molecules. Internally in molecule m, the localized spin moment $\mathbf{S}_m$ interacts with the electron spin $\mathbf{s}_m = \sum_{\sigma\sigma'} d^\dagger_{m\sigma} \boldsymbol{\sigma}_{\sigma\sigma'} d_{m\sigma'}/2$ via exchange

$$\mathcal{H}_{\rm int} = \sum_m v_m \mathbf{s}_m \cdot \mathbf{S}_m, \tag{3}$$

where v_m is the exchange integral, and we assume that $v_m = v$. We focus on the case with non-magnetic leads,

$$\mathcal{H}_{L/R} = \sum_{\mathbf{k}\sigma \in L/R} \varepsilon_{\mathbf{k}} c^\dagger_{\mathbf{k}\sigma} c_{\mathbf{k}\sigma}, \tag{4}$$

where $c^\dagger_{\mathbf{k}\sigma}$ creates an electron in the left (L; $\mathbf{k} = \mathbf{p}$) or right (R; $\mathbf{k} = \mathbf{q}$) lead at the energy $\varepsilon_{\mathbf{k}}$ and spin σ. Tunneling between the leads and molecules is described by

$$\mathcal{H}_T = \sum_{\mathbf{p}\sigma} T_L c^\dagger_{\mathbf{p}\sigma} d_{L\sigma} + \sum_{\mathbf{q}\sigma} T_R c^\dagger_{\mathbf{q}\sigma} d_{R\sigma} + H.c. \tag{5}$$

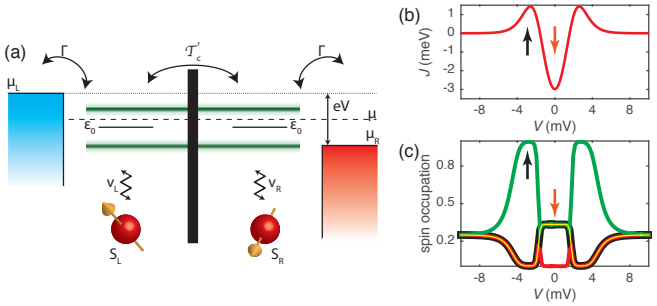

FIG. 1: (Color online) (a) Molecular dimer of paramagnetic molecules. An electron (at energy ε_0) in each molecule interacts with the localized spin moment ($\mathbf{S}_m$, $m = L,R$) via exchange (v_m) with the electron in the adjacent molecule (tunneling rate $\mathcal{T}_c$) and with electron sin the left/right electrode (coupling Γ). The left/right nonmagnetic electrode is characterized by its electrochemical potential ($\mu_{L/R}$). Effective molecular orbutals ($\varepsilon_0 \pm \mathcal{T}_c$) emerge from intermolecular tunneling. (b) Effective exchange interaction between the localized spin moments as function of the voltage bias V. (c) Occupation of the states in the spin dimer. The green curve represents the occupation of the lowest energy eigenstate of the spin dimer which changes character between spin singlet and spin triplet states as function of the voltage bias. Other colors analogously represent the occupation of the consecutively higher energy eigenstates. Around equilibrium three states are degenerate and from the spin triplet. Calculations have been made at $T = 4$ K for $\varepsilon_0 = 0$, $\mathcal{T}_c = 1$ meV, $v_m = 5$ meV, and $\Gamma = 1$, meV. In panels (b) and (c), the ferromagnetic and antiferromagnetic regimes of the spin dimer are indicated with red and black arrows, respectively.

and we define the voltage bias V across the junction by $eV = \mu_L - \mu_R$, where μ_χ, $\chi = L,R$, denotes the electrochemical potential of the lead χ.

In this way $\mathcal{H}_L + \mathcal{H}_R + \mathcal{H}_T + \mathcal{H}_M$ provides a spin-degenerate electronic structure which mediates the exchange interactions between the localized spin moments and the spin-degeneracy implies that these interactions are purely isotropic [55, 57], such that we retain the Heisenberg model only for the spins. More details will be discussed below.

A. Exchange interactions

It was shown previously that the effective interactions between the localized spins in the current set-up can be modelled by the Hamiltonian [57]

$$\mathcal{H}_S = \sum_{mn} \Big(J_{mn} \mathbf{S}_m \cdot \mathbf{S}_n + \mathbf{D}_{mn} \cdot [\mathbf{S}_m \times \mathbf{S}_n] + \mathbf{S}_m \cdot \mathbb{I}_{mn} \cdot \mathbf{S}_n \Big), \quad (6)$$

where the parameter J_{mn} denotes the isotropic Heisenberg interaction, whereas $\mathbf{D}_{mn}$ and $\mathbb{I}_{mn}$ respectively denotes the Dzyaloshinskii-Moriya and Ising interactions which both introduce anisotropic interactions into the system. In the present system, where the there is no spin-dependence imposed, either by external or internal forces, the anisotropic interactions vanish, $\mathbf{D}_{mn} = 0$, $\mathbb{I}_{mn} = 0$, and we retain the isotropic Heisenberg interaction only.

Here, we treat the spin dimer as an equilibrium system in the sense that we require a conserved number of particles for which the occupations of the states are given by the Gibbs distribution. This is a valid approximation for localized spins where the hybridization with the surrounding itinerant electrons is small such that nature of the localized electrons can be described in terms of a Kondo-like model rather than a fluctuating spin model in the sense of the Hubbard or Anderson models.

The spin-spin interactions are, nevertheless, influenced by the tunneling current that flows through the molecular complex. In such set-ups, the effective magnetic interaction parameter J between the two spins can be calculated using the expression, see Refs. [55, 57],

$$J = -\frac{\mathcal{T}_c^2}{8\pi} v^2 \sum_\chi \int \Gamma^\chi f_\chi(\omega)(\omega - \varepsilon_0) \frac{(\omega-\varepsilon_0)^2 - \mathcal{T}_c^2 - (\Gamma/8)^2}{|(\omega - \varepsilon_0 + i\Gamma/8)^2 - \mathcal{T}_c^2|^4} d\omega, \quad (7)$$

where $\Gamma = \sum_{\chi=L,R} \Gamma^\chi$, with $\Gamma^\chi = 2\pi \sum_{\mathbf{k}\sigma\in\chi} T_\chi^2 \delta(\omega - \varepsilon_{\mathbf{k}})$, is the coupling to the leads, and $f_\chi(\omega)$ is the Fermi function at the chemical potential μ_χ. Here, we have assumed that the molecular level $\varepsilon_m = \varepsilon_0$, $m = L,R$, which is reasonable for equivalent molecules.

The voltage bias dependence of J is plotted in Fig. 1 (b) for the case with $\varepsilon_0 = 0$ (for other parameters, see the figure caption). Near equilibrium ($V \approx 0$), $\mu_R \approx \mu_L = \mu$, this integral gives a negative (*ferromagnetic*) value for J, indicated by the red arrow in Fig. 1 (b), whenever μ lies between the upper and lower effective orbital energies $\varepsilon_0 \pm \mathcal{T}_c$ of the molecular dimer. In this regime the ground state of the spin dimer is a spin triplet, labelled by $|T;m = 0,\pm\rangle$ where T denotes the triplet and m its projection. This is illustrated in Fig. 1 (c), which shows the occupation number for the four possible states in the spin dimer corresponding to the evolution of J in panel (b). The red arrow indicates that the three projections of the spin triplet have equal occupation probability ($\sim 1/3$). With increasing voltage bias, μ_L and μ_R approach the orbital energies $\varepsilon_0 \pm \mathcal{T}_c$, which leads to a peaked positive (*anti-ferromagnetic*) J as $\mu_{L/R}$ sweeps through the orbital energies (indicated by the black arrow in Fig. 1 (b)). Hence, the spin dimer acquires a spin singlet ground state, $|S\rangle$, with nearly unit occupation probability, as is indicated by the black arrow in Fig. 1 (c). By further increasing the voltage bias, eventually both energies $\varepsilon_0 \pm \mathcal{T}_c$ lie between μ_L and μ_R and J remains positive but approaching zero (henceforth referred to as the *paramagnetic* regime), which leads to that the ground state of the spin dimer becomes a superposition of the four Fock states constituting the four dimensional Hilbert space. In this regime, where $J \to 0$, the four states acquire equal occupation probability ($\sim 1/4$), which can be seen in Fig. 1 (c). It should be emphasized, however, that the total magnetic moment of the spin dimer vanishes for all voltages due to the absence of magnetic anisotropies.

Next, we consider the influence of a temperature difference between the leads on the exchange interaction. The temperatures of the leads are included in the respective Fermi function on which the exchange interaction within the spin dimer de-

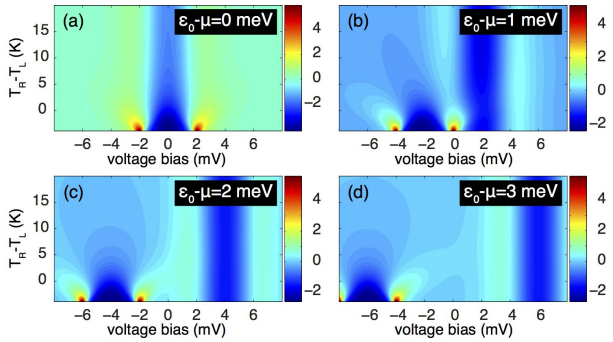

FIG. 2: (Color online) The exchange interaction J (units: meV) between the molecular spins as function of voltage bias V and temperature difference ΔT for different gating conditions, such that $\varepsilon_0 - \mu = 0, 1, 2, 3$ meV. Other parameters are as in Fig. 1.

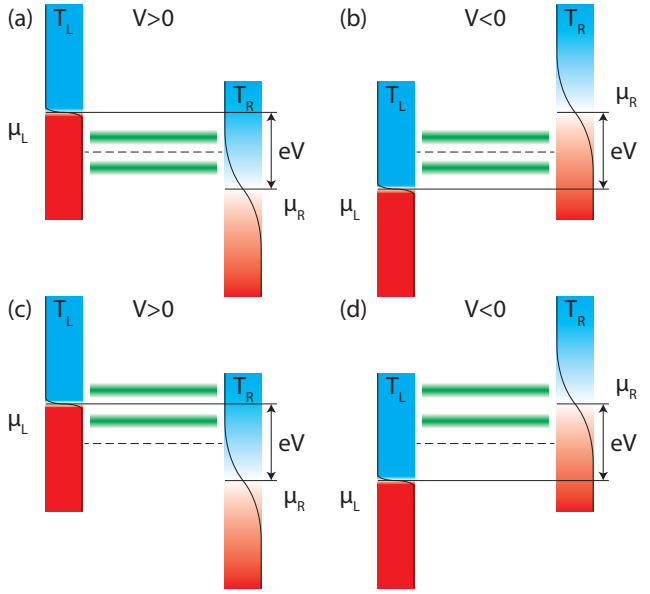

FIG. 3: (Color online) The combined role of the voltage bias and temperature difference on the tunneling conditions for (a), (c) positive and (b), (d) negative bias, and (a), (b) symmetric and (c), (d) asymmetric molecular orbitals around μ (dashed). The left (right) lead is defined at the temperature T_L (T_R) and chemical potential μ_L (μ_R); in the figure $T_L < T_R$ and $\mu_L - \mu_R = eV$. A low (high) temperature sustains a sharp (fuzzy) boundary between the occupied and unoccupied electron states in the metal.

pends, which is seen in Eq. (7). This dependence on the Fermi functions to the left and right suggests that the exchange not only varies as function of the temperature of the leads and the temperature difference between them but also the position of the energy levels with respect to the equilibrium chemical potential μ. The properties of the exchange interaction related to the temperature difference across the junction and the energy of the localized levels are illustrated in Fig. 2, which show the exchange interaction energy as function of the voltage bias and temperature difference for different energies $\varepsilon_0 - \mu$. There is a clear distinction between the situation in panel (a) compared to panels (b) – (d), which originates in the level position relative to μ.

First, whenever the localized level $\varepsilon_0 - \mu = 0$, the molecular bonding (at the energy: $\varepsilon_0 - \mathcal{T}_c$) and anti-bonding (at the energy: $\varepsilon_0 + \mathcal{T}_c$) orbitals are centered symmetrically around μ which leads to that the influences from the left and right leads is symmetric with respect to voltage bias and temperature difference. The situation is schematically depicted in Fig. 3 (a), (b). The first thing to notice is a weakening of the exchange interaction caused by the increased thermal spread of the electrons in the hot reservoir, compared to the cold reservoir. In equilibrium, then, in comparison to the cold reservoir the hot reservoir contains a larger number of electrons above and below both molecular orbitals which contribute to an anti-ferromagnetic interaction and simultaneously a smaller number of electrons that contribute to the ferromagnetic exchange. This results in a weaker ferromagnetic interaction and which is verified in the simulations, see Fig. 2 (a). The analogous argument holds for finite biases in the anti-ferromagnetic regime, however, utilized in the opposite way. Due to the thermal distribution of the electrons, there are electrons in the hot reservoir contributing to both the ferromagnetic and anti-ferromagnetic exchange which results in an effectively weaker anti-ferromagnetic exchange, see Fig. 2 (a). Moreover, since the thermal distribution of the electrons is symmetric around the pertinent chemical potential, the effect is equal regardless of the polarity of the voltage bias across the junction, which basically indicates voltage bias symmetric transport properties of the junction under these conditions.

Next, whenever the molecule is gated such that the localized level ε_0 is off-set from the chemical potential μ, a finite temperature difference do generate an asymmetry with respect to the voltage bias, see Fig. 2 (b) – (d). One can convince oneself that the exchange is symmetric with respect to the voltage bias at vanishing temperature difference, however, in general the asymmetry is conspicuous. Under the given conditions, $\varepsilon_0 - \mu > 0$ and variable T_R with $T_L = 4$ K fixed, the ferromagnetic regime at positive voltages remains nearly unaffected by changes in the temperature difference. This can be schematically understood from the sketch in Fig. 3 (c), showing μ_L lying between the molecular orbitals. Then, the narrow thermal spread of the electrons in the left lead maintains a strong contribution to the ferromagnetic exchange while the contribution from the right lead is negligible more or less independently of its temperature. By the same token one can understand that the ferromagnetic regime for negative voltages is extremely sensitive to the temperature of the right lead, see Fig. 3 (d). Under these conditions, the exchange interaction is dominated by the contribution from the right lead while the contribution from the left lead is negligible. Hence, at elevated temperatures there are competing contributions to the exchange of both ferromagnetic and anti-ferromagnetic nature which leads to a very weak ferromagnetic exchange that weakens with increasing temperature difference.

III. TRANSPORT FORMULAS

Here, we will briefly go through and summarize the approach we employ to study the transport properties governed by the molecular spin dimer. First, the current under interest are the heat and charge currents, which are defined as

$$I_Q = I_E - \mu I_N, \tag{8a}$$
$$I_c = -eI_N, \tag{8b}$$

respectively, where $I_{E(N)}$ denotes the energy (particle) current through the junction. Second, we notice that the energy and particle currents through the system are defined as the rate of change of the energy and the particle number, respectively. Despite that we consider stationary conditions in this article, we nonetheless need to derive the fluxes passing through both the left and the right interfaces. Concerning the particle flux, conservation of particles ensures that the rate of particles passing through one of the interfaces equals the corresponding rate at the other interface. However, the component in the heat current that is generated by the particle flux is not a conserved quantity [74], since this component is the product of the chemical potential and the particle flux. Hence, we need to address the fluxes at both interfaces. Fortunately, the expressions for the fluxes at the left and right interfaces are quite analogous which allows us to write them in a generic form. Accordingly, we calculate the energy and particle currents at the interface χ by

$$I_E^\chi = \frac{d}{dt}\langle \mathcal{H}_\chi\rangle = -2T_\chi \mathrm{Im}\sum_{\mathbf{k}\sigma}\varepsilon_{\mathbf{k}}(-i)F^<_{\mathbf{k}\chi\sigma}(t,t), \tag{9a}$$
$$I_N^\chi = \frac{d}{dt}\langle N_\chi\rangle = -2T_\chi \mathrm{Im}\sum_{\mathbf{k}\sigma}(-i)F^<_{\mathbf{k}\chi\sigma}(t,t), \tag{9b}$$

where we have defined the lesser form $F^<_{\mathbf{k}\chi\sigma}(t,t')$ of the transfer Green function (Green function) $F_{\mathbf{k}\chi\sigma}(t,t') = (-i)\langle \mathrm{T} c_{\mathbf{k}\sigma}(t) d^\dagger_{\chi\sigma}(t')\rangle$. Using standard theory [75] and restoring $\hbar$, the currents can be compactly written on the form

$$I_E^\chi = (-i)\frac{\Gamma^\chi}{\hbar}\mathrm{sp}\int \omega\Big(f_\chi(\omega)\mathbf{G}^>_\chi(\omega) + f_\chi(-\omega)\mathbf{G}^<_\chi(\omega)\Big)\frac{d\omega}{2\pi}, \tag{10a}$$
$$I_N^\chi = (-i)\frac{\Gamma^\chi}{\hbar}\mathrm{sp}\int \Big(f_\chi(\omega)\mathbf{G}^>_\chi(\omega) + f_\chi(-\omega)\mathbf{G}^<_\chi(\omega)\Big)\frac{d\omega}{2\pi}. \tag{10b}$$

Here, sp denotes the trace over spin 1/2 space whereas $\mathbf{G}^{</>}_\chi$, $\chi = L,R$, denotes the 2×2-matrix Green function of the molecule adjacent to the lead χ.

As we mentioned above, the stationary conditions imply that the particle currents I_N^L and I_N^R are equal up to their opposite signs, that is, $I_N^R = -I_N^L$. Then, since we shall express the total heat current using $I_Q = (I_E^L - \mu_L I_N^L)/2 - (I_E^R - \mu_R I_N^R)/2$, in turn, this leads to that the particle contribution to the heat current $(-(\mu_L I_N^L - \mu_R I_N^R)/2)$ can be written as $-(\mu_L+\mu_R)I_N^L/2 = -\mu I_N^L/2$. As we here measure all energies relative to the chemical potential μ, this will effectively be zero which means that the particle contribution to the heat current vanishes and we shall not have to consider its presence in the following.

We make further analytical progress by constructing an explicit expression for the Green function $\mathbf{G}_\chi$. To this end we include the broadening effects from the couplings to the leads as well as the inter-molecular tunneling and intra-molecular exchange interactions with the localized spin moments. These presumptions lead to that we can write the molecule projected retarded/advanced Green functions $\mathbf{G}_\chi$ as [55]

$$\mathbf{G}^{r/a}_{L(R)}(\omega) = \frac{1}{2\tilde{\mathcal{T}}_c}\sum_{s=\pm}\frac{\tilde{\mathcal{T}}_c\sigma^0 - 2sv\langle S^z_{R(L)}\rangle\sigma^z}{\omega - E_s \pm i\Gamma/8}, \tag{11}$$

where the excitation energies $E_\pm = \varepsilon_0 \pm \tilde{\mathcal{T}}_c/2$ and $\tilde{\mathcal{T}}_c^2 = v^2\langle S^z_L - S^z_R\rangle^2 + 4\mathcal{T}_c^2$.

The Green function $\mathbb{G}$ for the full dimer system is a 4×4-matrix $\mathbb{G} = \{\mathbf{G}_{\chi\chi'}\}_{\chi,\chi'=L,R}$, in which each entry is a 2×2-matrix $\mathbf{G}_{\chi\chi'} = \{G_{\chi\sigma\chi\sigma'}\}_{\sigma,\sigma'=\uparrow,\downarrow}$. Here, the subscripts χ,χ' refer to the left (right) molecule if $\chi\chi' = LL$ ($\chi\chi' = RR$) and coupling between the molecules for $\chi\chi' = LR$ or $\chi\chi' = RL$. For brevity, we write $\mathbf{G}_{\chi\chi} = \mathbf{G}_\chi$. Each entry is defined by

$$G_{\chi\sigma\chi'\sigma'}(z) = \langle\langle d_{\chi\sigma}|d^\dagger_{\chi'\sigma'}\rangle\rangle(z) = \int(-i)\langle \mathrm{T} d_{\chi\sigma}(t)d^\dagger_{\chi'\sigma'}(t')\rangle e^{-iz(t-t')}dt'. \tag{12}$$

The equation of motion for $\mathbb{G}$ can be summarized in the Dyson equation

$$\mathbb{G} = \mathbb{G}_0 + \mathbb{G}_0\mathbf{\Sigma}\mathbb{G}, \tag{13}$$

where $\mathbb{G}_0$ is the bare Green function for the coupled molecules, however, without couplings to the leads, whereas $\mathbf{\Sigma}$ defines the self-energy generated by the couplings to the leads. It can be noticed that since molecule 1 (2) only couples to the left (right) lead, the retarded form of this self-energy can be written as the diagonal matrix $\mathbf{\Sigma} = (-i)\mathrm{diag}\{\Gamma^L_\uparrow, \Gamma^L_\downarrow, \Gamma^R_\uparrow, \Gamma^R_\downarrow\}$. Considering spin-degenerate conditions, we can set $\Gamma^\chi_\sigma = \Gamma^\chi/2$. As an effect of the Dyson equation for $\mathbb{G}$, the corresponding lesser/greater forms are given by $\mathbb{G}^{</>} = \mathbb{G}^r\mathbf{\Sigma}^{</>}\mathbb{G}^a$, where the lesser/greater forms of the self-energy is given by

$$\mathbf{\Sigma}^{</>}(\omega) = (\pm i)\frac{1}{2}\begin{pmatrix} f_L(\pm\omega)\Gamma^L\sigma^0 & 0 \\ 0 & f_R(\pm\omega)\Gamma^R\sigma^0\end{pmatrix}. \tag{14}$$

When putting these results into the combination of the lesser and greater Green functions in the transport formulas, Eq. (10), we retain only

$$f_\chi(\omega)\mathbf{G}^>_\chi(\omega) - f_\chi(-\omega)\mathbf{G}^<_\chi(\omega) = (-i)\frac{\Gamma^R}{2}\Big(f_\chi(\omega) - f_{\chi'}(\omega)\Big)\mathbf{G}^r_{\chi\chi'}(\omega)\mathbf{G}^a_{\chi'\chi}(\omega), \tag{15}$$

out of which the only finite terms are the ones that couple the two molecules to one another and it is, therefore, necessary to study the forms of the site off-diagonal Green functions $\mathbf{G}_{LR}$ and $\mathbf{G}_{RL}$. By a straight forward calculation one finds that these

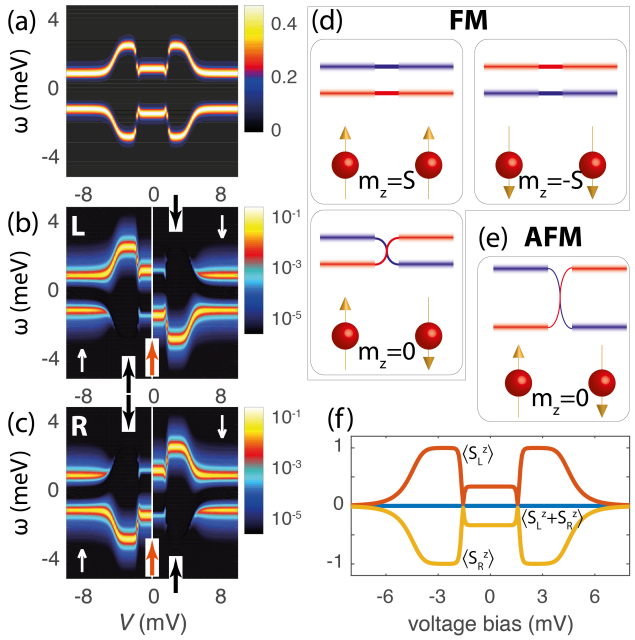

FIG. 4: (Color online) (a) Total density of electron states in the molecular dimer as function of the voltage bias. (b), (c) Molecule and spin projected (indicated by white arrows) densities of electron states of the left and right non-gated ($\mu = 0$) molecules, respectively, as function of the voltage bias V and energy ω. (d), (e) Schematic views of the back-action of the spin triplet (d) and spin singlet (e) configurations on the molecular orbitals. The spin triplet (singlet) generates as delocalized (localized) density of electron states resulting from the average of three degenerate (a single) spin configurations. (f) Molecule projected spin expectation values of the localized spins $\langle S^z_\chi\rangle$ and the total magnetic moment $\langle S^z_L + S^z_R\rangle$. Parameters are as in Fig. 1.

Green functions can be written as

$$\mathbf{G}^{r/a}_{\chi\chi'}(\omega) = \frac{\mathcal{T}_c}{2}\sum_{s=\pm}\frac{\sigma^0 - s\sigma^z}{\omega - \varepsilon_0 - sv\langle S^z_\chi\rangle \pm i\Gamma/8}\mathbf{G}^{r/a}_{\chi'}(\omega)$$
$$= \frac{\mathcal{T}_c}{4\tilde{\mathcal{T}}_c}\sum_{ss'=\pm}\frac{[\sigma^0 - s\sigma^z][\tilde{\mathcal{T}}_c\sigma^0 - 2s'v\langle S^z_\chi\rangle\sigma^z]}{[\omega - \varepsilon_0 - sv\langle S^z_\chi\rangle \pm i\Gamma/8][\omega - E_{s'} \pm i\Gamma/8]}. \quad (16)$$

We obtain a better understanding of the expected transport properties by considering the spin and molecule projected densities of electron states $\boldsymbol{\rho}_\chi(\omega) = -\mathrm{Im}\mathbf{G}_\chi(\omega)/\pi$. The total density of electron states of the dimer is shown in Fig. 4 (a), showing a significant variation of the energy position of the density as function of the voltage bias; bright ridges correspond to a high electron density. Here we have used the same conditions as in Fig. 1, which gives the ferromagnetic regime for voltage biases in the range -2 mV $< V < 2$ mV, followed by the anti-ferromagnetic regime at voltage biases between ±2 mV and ±4 mV and the paramagnetic regime in the range outside ±4 mV.

First we consider the energy shift of the density peaks between the ferromagnetic and anti-ferromagnetic regimes. The energies of the bonding and anti-bonding orbitals are given by $E_\pm = \varepsilon_0 \pm \tilde{\mathcal{T}}_c/2$. Assuming weak intermolecular tunneling $\mathcal{T}_c$, the renormalized tunneling rate $\tilde{\mathcal{T}}_c$ can be approximated by $\tilde{\mathcal{T}}_c \approx v\langle S^z_L - S^z_R\rangle + 2\mathcal{T}_c^2/v|\langle S^z_L - S^z_R\rangle|$, which leads to the energies $E_\pm \approx \varepsilon_0 \pm v|\langle S^z_L - S^z_R\rangle|/2$. The results in the ferromagnetic, anti-ferromagnetic and paramagnetic regimes are summarized in Table I. In the anti-ferromagnetic regime, on the one hand, the spins $\langle S^z_L\rangle = -\langle S^z_R\rangle = S$, see Fig. 4 (e), (f), which leads to an energy spacing of roughly $2vS$ between the bonding and anti-bonding orbitals. In the ferromagnetic regime, on the other hand, there is a three-fold degenerate set of configurations, see Fig. 4 (d), which leads to that the total expectation values $\langle S^z_\chi\rangle$ are reduced to $1/3$ of the values in the anti-ferromagnetic regime, see Fig. 4 (f), since the expectation values of the two parallel configurations exactly cancel. Therefore, the energy spacing between the bonding and anti-bonding orbitals becomes roughly $2vS/3$. In the paramagnetic regime the four states are four-fold degenerate, since the exchange interaction approaches zero, see Fig. 4 (f), which leads to that the spins are uncorrelated. The orbital energy separation is then governed by the intermolecular tunneling rate $\mathcal{T}_c$.

Remaining within the assumption of weak intermolecular tunneling, we find that the spectral weight of, for instance, the right molecule Green function contains the factor $\tilde{\mathcal{T}}_c\sigma^0 - 2s'v\langle S^z_L\rangle\sigma^z \approx v\langle S^z_L - S^z_R\rangle\sigma^0 - 2s'v\langle S^z_L\rangle\sigma^z$ in the numerator. Hence, for $s' = +$ and $s' = -$, the spectral weights are given by roughly $v\langle S^z_L + S^z_R\rangle$ and $v\langle 3S^z_L - S^z_R\rangle$, respectively. In the anti-ferromagnetic regime, the spins are anti-parallel such that $\langle S^z_L\rangle = -\langle S^z_R\rangle$ which leads to that the former spectral weight becomes negligible whereas the latter is finite. The implication of this distribution of the spectral weights can now be understood as a localization of the electronic density to the bonding (−) and anti-bonding (+) orbitals at the energies $E_\pm$. The density of electron states projected onto the left and right molecules can be written

$$\boldsymbol{\rho}_L(\omega) \approx \frac{\Gamma}{16\pi}\left(\frac{\sigma^0 + \sigma^z}{(\omega - E_+)^2 + (\Gamma/8)^2} + \frac{\sigma^0 - \sigma^z}{(\omega - E_-)^2 + (\Gamma/8)^2}\right), \quad (17a)$$

$$\boldsymbol{\rho}_R(\omega) \approx \frac{\Gamma}{16\pi}\left(\frac{\sigma^0 - \sigma^z}{(\omega - E_+)^2 + (\Gamma/8)^2} + \frac{\sigma^0 + \sigma^z}{(\omega - E_-)^2 + (\Gamma/8)^2}\right), \quad (17b)$$

showing the strong localization of the bonding and anti-bonding orbitals to i) opposite spin projections and ii) opposite molecules. From these densities we can establish the selection rule in the anti-ferromagnetic regime stating that the spin σ projection of the bonding (anti-bonding) orbital is localized in one molecule and the opposite spin projection in the

TABLE I: Orbital energies in the ferromagnetic, anti-ferromagnetic and independent regimes for small intermolecular tunneling.

	E_-	E_+	$E_+ - E_-$
AFM	$\varepsilon_0 - vS$	$\varepsilon_0 + vS$	$2vS$
FM	$\varepsilon_0 - vS/3$	$\varepsilon_0 + vS/3$	$2vS/3$
PM	$\varepsilon_0 - vS/4$	$\varepsilon_0 + vS/4$	$vS/2$

other. Under spin-conserving tunneling conditions between the molecules there is, hence, no elastic tunneling process that allows for tunneling between the molecules. It is therefore expected that the transport through the molecule in the anti-ferromagnetic regime is suppressed by at least $\mathcal{T}_c^2/v$, which in the case illustrated in Fig. 1 is expected to lead to a suppression of about $1/5$.

This result should be contrasted by the properties in the ferromagnetic regime. Again, we consider the approximate spectral weights $v\langle S_L^z + S_R^z\rangle$ and $v\langle 3S_L^z - S_R^z\rangle$ and again the latter spectral weight is finite just like in the anti-ferromagnetic regimes. The former spectral weight, on the other hand, is finite as well in the ferromagnetic regime. The implication of this distribution of the spectral weights being finite for both spin projections in both molecules is that the orbitals are delocalized which allows for elastic spin-conserving tunneling between the molecules. Regarding the transport properties a finite conductance should be expected in the ferromagnetic regime, which is significantly larger than in the anti-ferromagnetic regime, however, likely to be smaller than in the paramagnetic regime since the molecular orbitals are not fully delocalized.

In the paramagnetic regime, finally, the exchange interaction between the spins vanishes which leads to that the molecular orbitals are completely delocalized throughout the molecular structure, the molecules are fully conjugated. As the molecular orbitals can be viewed as independent conduction channels, the system can be addressed in a simple Landauer-Büttiker picture in which the conductance is limited only by the number of conduction channels in the junction.

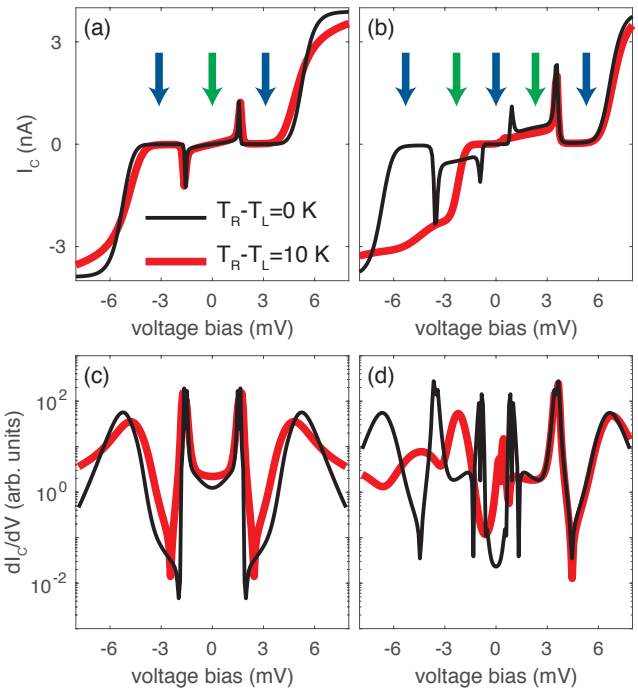

FIG. 5: (Color online) (a), (b), The charge current I_C (units: nA) and (c), (d), differential conductance dI_C/dV (arb. units) as function of voltage bias V for $T_R - T_L = 0$ (black – faint) and $T_R - T_L = 10$ K (red – bold) for (a), (c), $\varepsilon_0 - E_F = 0$ meV and (b), (d), $\varepsilon_0 - E_F = 1$ meV. Other parameters are as in Fig. 1. In panels (a) and (b), the ferromagnetic and anti-ferromagnetic regimes are indicated with green and blue arrows, respectively.

IV. RESULTS AND DISCUSSION

Regarding the charge transport across the junction, most of its properties can be understood in terms of the degree of delocalization of the electronic density in the molecular dimer. As we have discussed in the previous sections, the magnetic states and configurations lead to qualitatively distinct regimes of the electronic properties of the dimer, something that is conveyed over to the inherit transport properties of the molecular dimer. Accordingly, the conductance in the ferromagnetic regime is expected to better, or, higher than in the anti-ferromagnetic regime. This conjecture is based on the fact that in the anti-ferromagnetic regime the spin projected electronic density in the bonding state is strongly localized to one *or* the other molecule, see Fig. 4 (b),(c), and in the opposite fashion for the anti-bonding orbital. Therefore, an electron residing in one of the molecules has a nearly vanishing probability to tunnel over the other molecule which leads to a strongly suppressed conductance. In the ferromagnetic regime, however, the electronic density is more delocalized throughout the molecular dimer which allows for resonant tunneling between the molecules and, in turn, leads to an increased conductance. These features and disparities of the two magnetic regimes can be observed in the current, see Fig. 5 (a), (b), where we have plotted the charge current I_c as function of the voltage bias at zero temperature difference (black – faint) and $T_R - T_L = 10$ K (red – bold). Especially for vanishing temperature difference, the anti-ferromagnetic and ferromagnetic regimes (indicated by blue and green arrows, respectively) are strikingly separated by sharp current resonances which originates from a vanishing exchange between the spin. The absence of the exchange interaction leads to uncorrelated spins and a completely delocalized charge density in the molecular dimer, which allows for a large current flow in the same way as in the high voltage regime where $J \to 0$.

The corresponding (differential) conductances dI_C/dV are plotted in Fig. 5 (c), (d), showing in the same way the disparate properties of the currents in the anti-ferromagnetic and ferromagnetic regimes. It is interesting that the conductance in the anti-ferromagnetic regime is about one to two orders of magnitude smaller than in the ferromagnetic, which should allow for a clear distinction between the regimes in realistic measurements. We remark here that the differential conductances (both with respect to the voltage bias and temperature difference) shown in this article are calculated as the numerical derivatives of the currents, using a scheme which yields an error smaller than the fourth power in the grid point distance.

At zero temperature difference across the junction, the current-voltage characteristics is necessarily symmetric whenever then electronic structure of the molecular dimer are symmetrically distributed, as is the case we consider here. In-

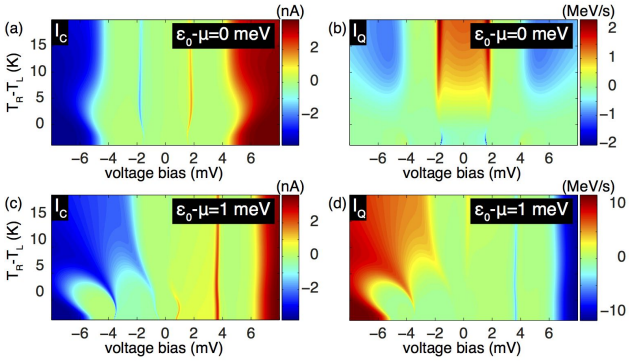

FIG. 6: (Color online) (a), (c), The charge current I_C (units: nA) and (b), (d), heat current I_Q (units: MeV/s) as function of voltage bias V and temperature difference $T_R - T_L$ for (a), (b), $\varepsilon_0 - E_F = 0$ meV and (c), (d), $\varepsilon_0 - E_F = 1$ meV. Other parameters are as in Fig. 1

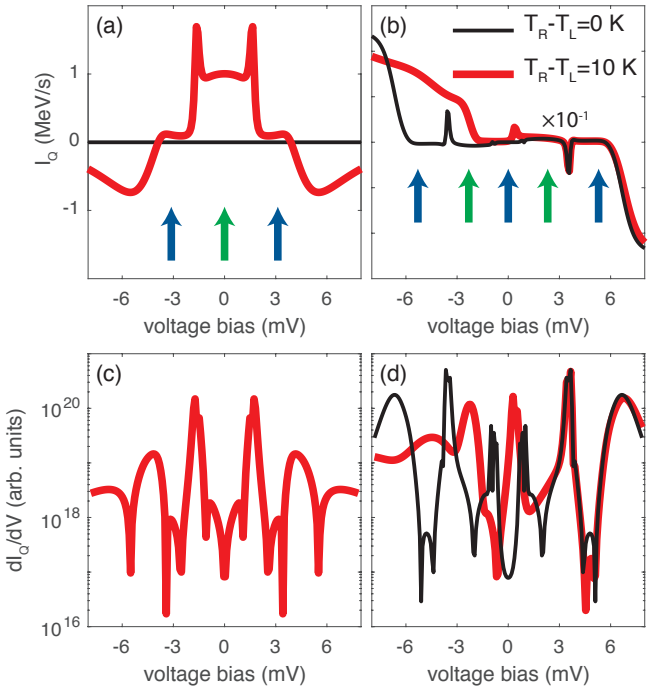

FIG. 7: (Color online) (a), (b), The heat current I_Q (units: MeV/s) and (c), (d), differential heat conductance dI_Q/dV (arb. units) as function of voltage bias V for $T_R - T_L = 0$ (black – faint) and $T_R - T_L = 10$ K (red – bold) for (a), (c), $\varepsilon_0 - E_F = 0$ meV and (b), (d), $\varepsilon_0 - E_F = 1$ meV. Other parameters are as in Fig. 1. In panels (a) and (b), the ferromagnetic and anti-ferromagnetic regimes are indicated with green and blue arrows, respectively. Notice that the currents plotted in panel (b) are an order of magnitude less than the actual currents.

troduction of a finite temperature difference changes this scenario, however, a necessary condition for breaking the symmetric current-voltage characteristics is that the bonding and anti-bonding orbitals do not surround μ symmetrically. This can be seen in the red – bold traces in Fig. 5. In panels (a) and (c), the molecular level $\varepsilon_0 = \mu$ which accordingly leads to a symmetric current as function of the voltage bias. In panels (b) and (d), in contrast, the molecular level satisfies $\varepsilon_0 - \mu = 1$ meV, which then generates a striking asymmetry in the current for finite temperature differences. This result can be traced back to the dramatically changed, weakened, exchange interaction between the spins which causes an increased degree of delocalization of the electronic density in the molecular dimer. In effect, therefore, both the ferromagnetic and anti-ferromagnetic regimes are essentially destroyed for negative voltages, see Fig. 5 (b) (red – bold). Hence, under the temperature difference between the leads the molecular dimer functions partially as a rectifying device where the magnetically active regimes can be employed in the forward direction while the system behaves like a normal conductor in the backward.

In Fig. 6 (a), (c), we show contour plots of the charge current as function of the voltage bias and temperature difference for (a) $\varepsilon_0 - \mu = 0$ meV and (c) $\varepsilon_0 - \mu = 1$ meV. The properties discussed in detail above can be seen to be verified in the larger picture, varying continuously with the variations of the external conditions. Especially in the latter case ($\varepsilon_0 - \mu = 1$ meV), the magnetically active regimes for negative voltage biases are seen to be destroyed already for small temperature differences, closely following the behavior of the exchange interactions, c.f., Fig. 2.

Next, in the discussion of the heat current, we again notice that most of the expected features can be explained in terms of the properties of the electronic structure in the molecular dimer analogous as with the charge current. However, for vanishing temperature difference between the leads a clear distinction compared to the charge current is that the finiteness of the heat current strongly depends on the energy of the localized level in the molecular assembly. This can be traced back to the product of the energy and the distribution functions ($\mathbf{G}_\chi^{<,>}$) of the molecular dimer in, for instance, Eq. (10a). One can make a simple comparison between the qualitative properties of the two currents by assuming a Lorentzian model, $1/[(\omega + \mu - \varepsilon_0)^2 + (\Gamma/2)^2]$, for the device embedded between the leads at low temperatures. Then, under the voltage bias $\mu_{L/R} = \mu \pm eV/2$, the two currents behave as

$$I_c \sim \frac{1}{\Gamma/2}\left(\arctan\frac{eV/2-\varepsilon_0}{\Gamma/2} + \arctan\frac{eV/2+\varepsilon_0}{\Gamma/2}\right), \tag{18a}$$

$$I_Q \sim \frac{1}{2}\ln\frac{(eV/2-\varepsilon_0)^2+(\Gamma/2)^2}{(eV/2+\varepsilon_0)^2+(\Gamma/2)^2} + \frac{\varepsilon_0-\mu}{\Gamma/2}\left(\arctan\frac{eV/2-\varepsilon_0}{\Gamma/2} + \arctan\frac{eV/2+\varepsilon_0}{\Gamma/2}\right). \tag{18b}$$

Hence, while both charge and heat currents has a normal on-set associated with the position of ε_0, described by the arctan-component, the heat current is also logarithmically resonant at ε_0. In addition, for the heat current the on-set at ε_0 is weighted by the position of ε_0 relative to μ and, therefore, this contribution to the heat current is expected to the small whenever ε_0 lies in the vicinity of μ. The logarithmic contribution tends to be small for large voltage biases, since it leads to an increas-

ingly symmetric argument, and is accordingly only significant for voltages such that either $eV/2-\varepsilon_0$ or $eV/2+\varepsilon_0$ is small.

Extrapolating this discussion to our present case with the molecular dimer, we can verify these expected features under the conditions of vanishing temperature difference. This can be be seen in Fig. 7 (a), (b) (black – faint). At $\varepsilon_0-\mu=0$, panel (a), the heat current is identically zero while a finite off-set from μ, panel (b), yields a finite heat current. In the latter case, the heat current is small in the magnetically active regime and grows large only at large voltages where the exchange interaction vanishes. Despite being small, however, there are strong variations in the heat current which are more clearly seen in the differential conductance, Fig. 7 (d) (black – faint). Consistently with the charge conductance, the heat conductance is lower in both anti-ferromagnetic and ferromagnetic regimes compared to the paramagnetic. The variations in the heat conductance stretches over more than four orders of magnitude, which is also consistent with the variations in the charge conductance. However, while the charge conductance in the ferromagnetic regime is significantly larger than in the anti-ferromagnetic, the heat conductance is more or less the same in the two regimes. In fact, it can be seen that the larger heat conductance can be correlated only with the crossover between anti-ferromagnetic and ferromagnetic, and anti-ferromagnetic and paramagnetic regimes. Hence, despite that the electronic density in the molecular dimer is less localized in the ferromagnetic regime compared to the anti-ferromagnetic, and despite this feature yields a significant difference in the charge current, the heat tends to be efficiently transmitted only when the molecular dimer is in its fully conjugated state, that is, when the exchange interaction is small.

The reason for this qualitative difference between the charge and heat currents, see Eq. (18), can be found in the properties of the two currents in the ferromagnetic regimes. In particular, the logarithmically resonant contribution to the heat current, which is absent in the charge current, peaks near the energies of the molecular bonding and anti-bonding orbitals, something which occurs within the ferromagnetic but not in the anti-ferromagnetic regime. Thereto, these resonant peaks are oppositely directed compared to the normal arctan contributions. Because of this resonant reduction, the total heat conductance is therefore in the ferromagnetic regime comparable to the conductance in the anti-ferromagnetic regime.

As for the heat current under finite temperature difference between the leads, see Fig. 7 (red – bold) and Fig. 6 (b), (d), this behavior is verified, although the variations of the heat current and corresponding conductance between the ferromagnetic and anti-ferromagnetic regimes are larger, see in particular Fig. 7 (d). This feature can, nonetheless, be traced back to an increased degree of delocalization in the ferromagnetic regime due to the increased thermal broadening from the hotter reservoir.

In the case where the localized level is off-set from μ, there is an interesting observation to be made in the temperature and voltage dependence of both the charge and heat currents. At finite temperature difference and voltage bias, there is a strong asymmetry with respect to zero voltage which is clear

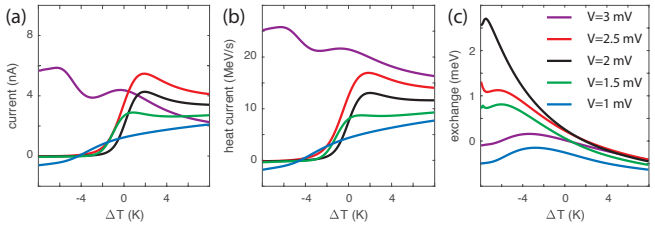

FIG. 8: (Color online) Thermal rectification. (a) Charge, (b) heat currents, and (c) exchange interaction, as function of the temperature difference for different voltage biases. Here, $\varepsilon_0-\mu=2$ and $\mathcal{T}_c=3$ meV, while other parameters are as in Fig. 1.

signature that the magnetically active dimer potentially can be used for current rectification. Previously it was shown in Ref. [55] that the charge current can be rectified by introducing a level off-set between the localized levels in the two molecules, something which possibly can be obtained by using different types of molecules. The asymmetry induced by the temperature difference provides a different mechanism to rectification which is also viable for the heat current. Indeed, the plots in Fig. 6 (c), (d), illustrate that both the charge and the heat current is rectified at finite temperature differences upon changing the polarity of the voltage bias. For this to be successful, the dimer has to be set-up with a finite level off-set from μ and a finite voltage bias. Moreover, the parameters of the molecular dimer have to be tuned such that the off-set between the bonding and anti-bonding orbitals is larger than the thermal energy fed into the dimer from the hotter electrode. This enables a crossover from the anti-ferromagnetic regime to either the ferromagnetic or paramagnetic regime, under changes in the temperature difference, which leads to strong variations in the currents. In principle, the stronger anti-ferromagnetic exchange one can obtain for one polarity of the temperature difference and the weaker the exchange can be in the opposite, regardless of sign, the larger the ratio between the currents for the two polarities. In Fig. 8 we plot the (a) charge and (b) heat current as function of the temperature difference for different voltage biases. We apply half the difference to the temperature in each lead such that $T_L=T-\Delta/2$ and $T_R=T+\Delta/2$, where the base temperature $T=4$ K. The calculations confirm the argument that variations of the exchange interaction from strongly anti-ferromagnetic to weakly ferromagnetic [$V\approx 2$ mV, see Fig. 2 (c)] indeed yields the larger ratio between the large and small current regimes.

Finally, we briefly discuss the differential conductances, both charge and heat conductances and with respect to both voltage bias and temperature difference. Hence, we calculate $\partial I_x/\partial V$ and $\partial I_x/\partial\Delta T$, where $x=c,Q$, see Figs. 9 (a) – (d) and 10 (a) – (d). In Figs. 9 and 10 we plot $\operatorname{arcsinh}\mathcal{F}$, where $\mathcal{F}$ is one of $\partial I_x/\partial V$, $\partial I_x/\partial\Delta T$, and S_x, in order to lower the values of the high amplitudes. First we notice that both currents have ranges with fairly rapid variations with the voltage bias and with the temperature difference. While these properties can be traced back to the corresponding variations of the exchange interaction, we can predict a few consequences

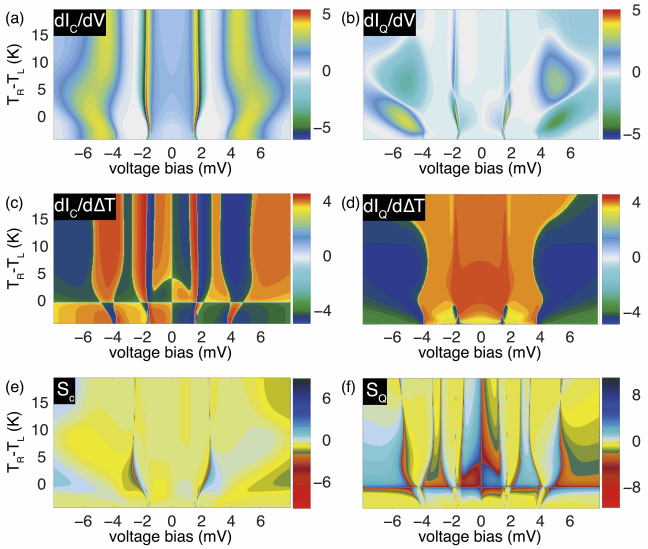

FIG. 9: (Color online) (a) – (d) Charge (a), (c), and heat (b), (d), conductances as differential derivatives with respect to the voltage bias (a), (b), and temperature difference (c), (d). (e), (f), Seebeck coefficients associated with the (e) charge, S_c, and (f) heat, S_Q, currents. Here, $\varepsilon_0 - \mu = 0$, while other parameters are as in Fig. 1. All contours show $\operatorname{arcsinh}\mathcal{F}$, where $\mathcal{F}$ is one of $\partial I_x/\partial V$, $\partial I_x/\partial \Delta T$, and S_x.

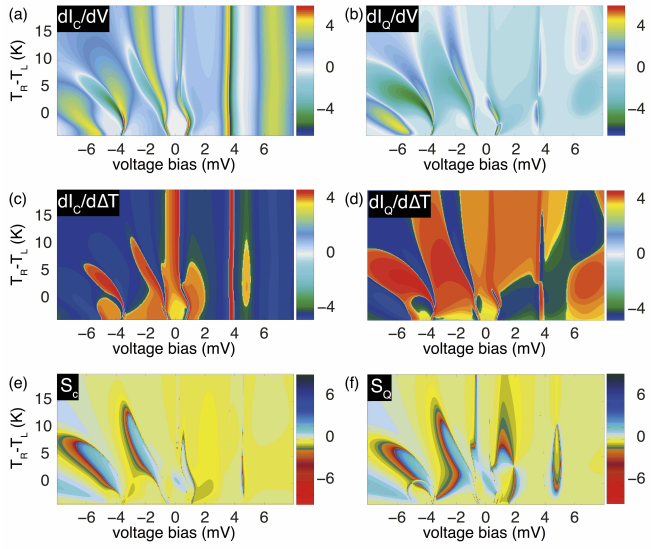

FIG. 10: (Color online) (a) – (d) Charge (a), (c), and heat (b), (d), conductances as differential derivatives with respect to the voltage bias (a), (b), and temperature difference (c), (d). (e), (f), Seebeck coefficients associated with the (e) charge, S_c, and (f) heat, S_Q, currents. Here, $\varepsilon_0 - \mu = 1$, while other parameters are as in Fig. 1. All contours show $\operatorname{arcsinh}\mathcal{F}$, where $\mathcal{F}$ is one of $\partial I_x/\partial V$, $\partial I_x/\partial \Delta T$, and S_x.

of these features on the ratios of the differential conductance with respect to the temperature difference and the differential conductance with respect to the voltage bias, that is,

$$S_c = -\frac{\partial I_c/d\Delta T}{\partial I_c/dV}, \tag{19}$$

where the notation S_c stands for the Seebeck coefficient [72], or, thermopower. Hence, as rapid variations in the charge current yield a large corresponding conductance and, oppositely, slow variations lead to a small conductance, we would expect that the Seebeck coefficient typically is large in the regions with weak variations of the charge current. One is therefore led to think that the Seebeck might be large in the anti-ferromagnetic regime since the current is both small and slowly varying with the voltage bias in those regimes, see Figs. 9 (a) and 10 (a). In addition, within the anti-ferromagnetic regimes, $\partial I_c/\partial \Delta T$ varies rapidly, including possible sign changes, near zero temperature difference between the leads. This conjecture is fairly well corroborated in the plots of the Seebeck coefficient shown in Figs. 9 (e) and 10 (e). In particular, it can be noticed in Fig. 9 (e) that the thermopower acquires large values in the anti-ferromagnetic regime (voltages roughly in the ranges $(-4,-2)$ and $(2,4)$ mV) for temperature differences between 0 K and 5 K. Except for these small regions of large thermopower, it tends to be small in the remainder of the magnetically active regimes although not vanishing. In the case with a finite level off-set, Fig. 10 (e), however, the thermopower tends to be large in the regions where the anti-ferromagnetic coupling is destroyed by the increased temperature difference. There are clearly visible domains at negative voltages which can be correlated with the cross over between the anti-ferromagnetic and paramagnetic regimes. At positive voltages where the dimer remains magnetically active in a larger temperature range, the thermopower is again small. We conclude that the thermopower in both the ferromagnetic and anti-ferromagnetic regimes is small and typically becomes finite at the crossovers to the paramagnetic regime. Hence, the spin-spin interaction provides a way to not only control the charge current but also the thermopower in the system.

In analogy with the definition of the Seebeck coefficient S_c associated with the charge current, we can define a coefficient S_Q for the heat current through

$$S_Q = -\frac{\partial I_Q/d\Delta T}{\partial I_Q/dV}. \tag{20}$$

Although we cannot give this coefficient an as simple interpretation as with the thermopower, we nevertheless find it useful in the analysis of the influence of the magnetic configurations on the thermal properties. It can be seen in Figs. 9 (b) and 10 (b) that the differential heat conductance, with respect to the voltage bias, has a non-trivial dependence on the voltage bias and temperature bias. Moreover, the dependence on the temperature difference is intriguing. We can, however, notice regarding the generic features of the heat Seebeck coefficient that its more or less vanishing in the magnetically active regimes except in the crossover between the different regimes, where the heat current varies slowly with the voltage bias but not necessarily with the temperature difference. The qualitative difference of the heat current compared to the charge current in the ferromagnetic regime, leads to that the

heat Seebeck coefficient provides a complimentary piece of information about the system under investigation in addition to the Seebeck coefficient.

V. SUMMARY

In summary we have studied a dimer of paramagnetic molecules with localized spins and its transport properties with respect to the charge and heat currents. We have shown that the voltage and temperature difference dependent exchange interaction between the localized spins leads to specific properties of the charge and heat currents. Particularly, the currents are generically larger in the ferromagnetic and paramagnetic regimes compared to the anti-ferromagnetic regimes. Qualitative differences between the charge and heat currents are noticed in the ferromagnetic regimes since the heat current comprises a resonant component which tends to reduce the total heat current as the bonding or anti-bonding orbitals of the molecular dimer approaches resonant conditions with the chemical potential of one of the leads. We also showed that the thermopower, Seebeck coefficient, is large in the anti-ferromagnetic regimes while the corresponding ratio for the heat current has a complimentary sensitivity to the transport properties which may be useful for analyses of the internal properties of the system.

Acknowledgments

We thank S. Borlenghi Garoia, A. Bouhon, K. Björnson, H. Hammar, D. Kuzmanovksi and Johan Schmidt for fruitful discussions. Financial support from Colciencias (Colombian Administrative Department of Science, Technology and Innovation) and Vetenskapsrådet is acknowledged.

[1] K. Huang, *Statistical Mechanics*, 2nd ed. (Wiley, 1987).
[2] A. Nitzan, Science (New York, N.Y.) **317**, 759 (2007).
[3] J. P. Pekola, Nature Physics **11**, 118 (2015).
[4] P. Reddy, S.-y. Jang, R. a. Segalman, and A. Majumdar, Science (New York, N.Y.) **315**, 1568 (2007).
[5] A. R. Garrigues, L. Wang, E. del Barco, and C. A. Nijhuis, Nature Communications **7**, 11595 (2016).
[6] E. A. Osorio, K. Moth-Poulsen, H. S. J. Van Der Zant, J. Paaske, P. Hedegå rd, K. Flensberg, J. Bendix, and T. Björnholm, Nano Letters **10**, 105 (2010), arXiv:0912.2640 .
[7] J. M. R. Parrondo, J. M. Horowitz, and T. Sagawa, Nature Physics **11**, 131 (2015), arXiv:0903.2792 .
[8] A. Bruch, M. Thomas, S. Viola Kusminskiy, F. Von Oppen, and A. Nitzan, Physical Review B - Condensed Matter and Materials Physics **93**, 1 (2016), arXiv:1511.03276 .
[9] M. Esposito, M. A. Ochoa, and M. Galperin, Physical Review Letters **114**, 1 (2015), arXiv:1411.1800 .
[10] A. Shastry and C. A. Stafford, **85721** (2016), 10.1103/PhysRevB.94.155433, arXiv:1603.00096 .
[11] T. Dauxois and M. Peyrard, *Cambridge University Press 2006*, 1 (Cambridge University Press, Cambridge, 2006) arXiv:arXiv:1011.1669v3 .
[12] C. K. Chiang, C. R. Fincher, Y. W. Park, A. J. Heeger, H. Shirakawa, E. J. Louis, S. C. Gau, and A. G. MacDiarmid, Physical Review Letters **39**, 1098 (1977).
[13] C. J. Fincher, D. Peebles, A. Heeger, M. Druy, Y. Matsumura, A. MacDiarmid, H. Shirakawa, and S. Ikeda, Solid State Communications **27**, 489 (1978).
[14] W. P. Su, J. R. Schrieffer, and A. J. Hegger, Physical Review B **22**, 2099 (1980).
[15] J. Rammer and H. Smith, Reviews of Modern Physics **58**, 323 (1986).
[16] A. J. Heeger, S. Kivelson, J. R. Schrieffer, and W. P. Su, Reviews of Modern Physics **60**, 781 (1988).
[17] S. Roth, H. Bleier, and W. Pukacki, Faraday Discussions of the Chemical Society **88**, 223 (1989).
[18] M. Nakata, M. Taga, and H. Kise, Polymer Journal **24**, 437 (1992).
[19] Y. Meir and N. S. Wingreen, Physical Review Letters **68**, 2512 (1992).
[20] Z. Bao, A. J. Lovinger, and A. Dodabalapur, Applied Physics Letters **69**, 3066 (1996).
[21] G. Parthasarathy, P. E. Burrows, V. Khalfin, V. G. Kozlov, and S. R. Forrest, Applied Physics Letters **72**, 2138 (1998).
[22] G. Chen and a. Shakouri, Journal of Heat Transfer **124**, 242 (2002).
[23] G. Chen and G. Chen, Applied Physics Letters **29**, 1 (2003).
[24] M. Haibo and U. Schollwock, Journal of Physical Chemistry A **113**, 1360 (2009), arXiv:0809.3211 .
[25] H. J. Haug and A.-P. Jauho, *Spinger Series in Solid State Sciences*, 2nd ed. (Springer, Berlin, 2008) arXiv:arXiv:1011.1669v3 .
[26] F. Giazotto, T. T. Heikkilä, A. Luukanen, A. M. Savin, and J. P. Pekola, Reviews of Modern Physics **78**, 217 (2006), arXiv:0508093 [cond-mat] .
[27] Y. Dubi and M. Di Ventra, Reviews of Modern Physics **83**, 131 (2011), arXiv:0910.0425 .
[28] Y. S. Liu and Y. C. Chen, Physical Review B - Condensed Matter and Materials Physics **79**, 6 (2009), arXiv:0812.0400 .
[29] M. F. Ludovico, J. S. Lim, M. Moskalets, L. Arrachea, and D. Sánchez, Physical Review B - Condensed Matter and Materials Physics **89**, 1 (2014).
[30] L. Arrachea and M. Moskalets, Physical Review B - Condensed Matter and Materials Physics **74**, 1 (2006), arXiv:0607278 [cond-mat] .
[31] M. Esposito, M. A. Ochoa, and M. Galperin, Physical Review B - Condensed Matter and Materials Physics **92**, 1 (2015), arXiv:1408.3608 .
[32] A. M. Daré and P. Lombardo, Physical Review B - Condensed Matter and Materials Physics **93**, 1 (2016), arXiv:1509.05606 .
[33] L. Arrachea, N. Bode, and F. Von Oppen, Physical Review B - Condensed Matter and Materials Physics **90**, 1 (2014), arXiv:1407.3127 .
[34] H. Zhou, J. Thingna, P. Hänggi, J.-S. Wang, and B. Li, Scientific reports **5**, 14870 (2015), arXiv:1505.06132 .
[35] D. Segal and B. K. Agarwalla, arXiv.org , arXiv:1506.08936v1 (2015), arXiv:1506.08936v1 .
[36] L. Ye, X. Zheng, Y. Yan, and M. Di Ventra, Physical Review B **94**, 245105 (2016), arXiv:1608.07760 .
[37] A. J. White, U. Peskin, and M. Galperin, Physical Review B

88, 205424 (2013).
[38] F. G. Eich, M. Di Ventra, and G. Vignale, Physical Review B - Condensed Matter and Materials Physics **93**, 1 (2016), arXiv:arXiv:1601.07807v1 .
[39] R. Q. Wang, L. Sheng, R. Shen, B. Wang, and D. Y. Xing, Physical Review Letters **105**, 1 (2010).
[40] J. P. Ramos-Andrade, O. Ávalos-Ovando, P. A. Orellana, and S. E. Ulloa, **155436**, 1 (2016), arXiv:1608.02046 .
[41] H. S. Kim, Z. M. Gibbs, Y. Tang, H. Wang, and G. J. Snyder, APL Materials **3**, 1 (2015).
[42] A. Crépieux, F. Åimkovic, B. Cambon, and F. Michelini, Physical Review B - Condensed Matter and Materials Physics **83**, 1 (2011), arXiv:1012.0658 .
[43] J. P. Bergfield and C. A. Stafford, Nano Letters **9**, 3072 (2009).
[44] M. Koole, J. M. Thijssen, H. Valkenier, J. C. Hummelen, and H. S. J. V. D. Zant, Nano Letters **15**, 5569 (2015).
[45] M. Koole, J. M. Thijssen, H. Valkenier, J. C. Hummelen, and H. S. J. V. D. Zant, Nano Letters **15**, 5569 (2015).
[46] H. Valkenier, C. M. Guédon, T. Markussen, K. S. Thygesen, S. J. van der Molen, and J. C. Hummelen, Physical Chemistry Chemical Physics **16**, 653 (2014).
[47] D. Fracasso, H. Valkenier, J. C. Hummelen, G. C. Solomon, and R. C. Chiechi, Journal of the American Chemical Society **133**, 9556 (2011).
[48] S. V. Aradhya, J. S. Meisner, M. Krikorian, S. Ahn, R. Parameswaran, M. L. Steigerwald, C. Nuckolls, and L. Venkataraman, Nano Letters **12**, 1643 (2012).
[49] C. Guédon, H. Valkenier, T. Markussen, K. Thygesen, J. Hummelen, and S. van der Molen, Nature Nanotechnology **7**, 305 (2012), arXiv:1108.4357 .
[50] T. Markussen and K. S. Thygesen, Physical Review B **89**, 085420 (2014).
[51] C. Bessis, M. L. D. Rocca, C. Barraud, P. Martin, J. C. Lacroix, and T. Markussen, Scientific Reports **6**, 20899 (2016).
[52] C. Bessis, M. L. D. Rocca, C. Barraud, P. Martin, J. C. Lacroix, and T. Markussen, Scientific Reports **6**, 20899 (2016).
[53] C. Guédon, H. Valkenier, T. Markussen, K. Thygesen, J. Hummelen, and S. van der Molen, Nature Nanotechnology **7**, 305 (2012), arXiv:1108.4357 .
[54] N. Darwish, I. Díez-Pérez, P. Da Silva, N. Tao, J. J. Gooding, and M. N. Paddon-Row, Angewandte Chemie - International Edition **51**, 3203 (2012).
[55] T. Saygun, J. Bylin, H. Hammar, and J. Fransson, Nano Letters **16**, 2824 (2016).
[56] S. Díaz and Á. S. Núñez, Journal of physics. Condensed matter : an Institute of Physics journal **24**, 116001 (2012).
[57] J. Fransson, J. Ren, and J.-x. Zhu, Physical Review Letters **113**, 257201 (2014), arXiv:1401.5592 .
[58] J. Fransson and J. X. Zhu, New Journal of Physics **10** (2008), 10.1088/1367-2630/10/1/013017, arXiv:0609673 [arXiv:cond-mat] .
[59] H. Hammar and J. Fransson, Physical Review B - Condensed Matter and Materials Physics **054311**, 1 (2016), arXiv:1603.03628 .
[60] N. a. Zimbovskaya, *Transport Properties of Molecular Junctions*, Vol. 254 (Springer, New York, 2013).
[61] M. Moskalets and G. Haack, physica status solidi (2016), arXiv:1609.04544 .
[62] B. Gaury, J. Weston, M. Santin, M. Houzet, C. Groth, and X. Waintal, Physics Reports **534**, 1 (2014), arXiv:arXiv:1307.6419v4 .
[63] N. A. Zimbovskaya, Journal of Physics: Condensed Matter **28**, 183002 (2016).
[64] R. W. Simmonds, Nature **492**, 358 (2012).
[65] B. W. Heinrich, L. Braun, J. I. Pascual, and K. J. Franke, Nature Physics **9**, 765 (2013).
[66] B. W. Heinrich, G. Ahmadi, V. L. Müller, L. Braun, J. I. Pascual, and K. J. Franke, Nano Letters **13**, 4840 (2013).
[67] B. W. Heinrich, L. Braun, J. I. Pascual, and K. J. Franke, Nano Letters **15**, 4024 (2015).
[68] I. E. Brumboiu, S. Haldar, J. Lüder, O. Eriksson, H. C. Herper, B. Brena, and B. Sanyal, Journal of Chemical Theory and Computation **12**, 1772 (2016).
[69] M. Urdampilleta, S. Klyatskaya, J.-P. Cleuziou, M. Ruben, and W. Wernsdorfer, Nature Materials **10**, 502 (2011), arXiv:1304.6543 [cond-mat.mes-hall] .
[70] R. Vincent, S. Klyatskaya, M. Ruben, W. Wernsdorfer, and F. Balestro, Nature **488**, 357 (2012).
[71] Z. F. Liu, S. Wei, H. Yoon, O. Adak, I. Ponce, Y. Jiang, W. D. Jang, L. M. Campos, L. Venkataraman, and J. B. Neaton, Nano Letters **14**, 5365 (2014).
[72] J. Fransson and M. Galperin, Physical chemistry chemical physics : PCCP **13**, 14350 (2011).
[73] M. Misiorny, M. Hell, and M. R. Wegewijs, Nature Physics **9**, 801 (2013), arXiv:arXiv:1407.5273v1 .
[74] M. Galperin, A. Nitzan, and M. A. Ratner, Physical Review B - Condensed Matter and Materials Physics **75**, 1 (2007), arXiv:0611169 [cond-mat] .
[75] A. P. Jauho, N. S. Wingreen, and Y. Meir, Physical Review B **50**, 5528 (1994), arXiv:9404027 [cond-mat] .